Impaired fatty acid import or catabolism in macrophages restricts intracellular growth of *Mycobacterium tuberculosis*

Nelson V. Simwela[1], Eleni Jaecklein [2], Christopher M. Sassetti[2], David G. Russell[1]*

1. Department of Microbiology and Immunology, College of Veterinary Medicine, Cornell University, Ithaca, New York, USA
2. Department of Microbiology, UMass Chan Medical School, Worcester, Massachusetts, USA

*Correspondence: dgr8@cornell.edu

Abstract

Mycobacterium tuberculosis (*Mtb*) infection of macrophages reprograms cellular metabolism to promote lipid retention. While it is clearly known that intracellular *Mtb* utilize host derived lipids to maintain infection, the role of macrophage lipid processing on the bacteria's ability to access the intracellular lipid pool remains undefined. We utilized a CRISPR-Cas9 genetic approach to assess the impact of sequential steps in fatty acid metabolism on the growth of intracellular *Mtb*. Our analyzes demonstrate that mutated macrophages that cannot either import, store or catabolize fatty acids restrict *Mtb* growth by both common and divergent anti-microbial mechanisms, including increased glycolysis, increased oxidative stress, production of pro-inflammatory cytokines, enhanced autophagy and nutrient limitation. We also show that impaired macrophage lipid droplet biogenesis is restrictive to *Mtb* replication, but increased induction fails to rescue *Mtb* growth. Our work expands our understanding of how host fatty acid homeostasis impacts *Mtb* growth in the macrophage.

Key words: Macrophages, *Mycobacterium tuberculosis*, lipid metabolism, CRISPR-Cas9, nutritional immunity

59 **Introduction**

60 *Mycobacterium tuberculosis* (*Mtb*), the causative agent of tuberculosis (TB), has caused disease
61 and death in humans for centuries (WHO, 2023). *Mtb* primarily infects macrophages in the lung
62 (Cohen et al., 2018; Wolf et al., 2007) wherein the bacterium relies on host derived fatty acids
63 and cholesterol for synthesis of its lipid rich cell wall, and to produce energy and virulence factors
64 (Peyron et al., 2008; Russell et al., 2009; Singh et al., 2012; Daniel et al., 2011; Muñoz-Elías and
65 McKinney, 2005; Pandey and Sassetti, 2008; Brzostek et al., 2009). Within the lung
66 microenvironment, resident alveolar macrophages preferentially oxidize fatty acids and are more
67 permissive to *Mtb* growth while recruited interstitial macrophages are more glycolytic and
68 restrictive of *Mtb* replication (Huang et al., 2018; Pisu et al., 2020; Pisu et al., 2021). Globally, *Mtb*
69 infection modifies macrophage metabolism in a manner that enhances its survival. *Mtb* infected
70 macrophages shift their mitochondrial substrate preference to exogenous fatty acids which drives
71 the formation of foamy macrophages that are laden with cytosolic lipid droplets (Peyron et al.,
72 2008; Russell et al., 2009; Cumming et al., 2018; Singh et al., 2012; Podinovskaia et al., 2013).
73 Foamy macrophages are found in abundance in the central and inner layers of granulomas, a
74 common histopathological feature of human TB (Russell et al., 2009; Kim et al., 2010).
75 Interference with key regulators of lipid homeostasis, such as the miR-33 and the transcription
76 factors peroxisome proliferator-activated receptor α (PPARα) and PPAR-γ enhances macrophage
77 control of *Mtb* (Kim et al., 2017; Almeida et al., 2009; Ouimet et al., 2016). Moreover, compounds
78 which modulate lipid metabolism such as the anti-diabetic drug metformin and some cholesterol
79 lowering drugs are under investigation for host directed therapeutics (HDTs) against *Mtb* (Parihar
80 et al., 2014; Singhal et al., 2014). Although the dependence of intracellular *Mtb* on host fatty acids
81 and cholesterol is well documented (Wilburn et al., 2018), the impact of specific aspects of
82 macrophage lipid metabolism on the bacteria remains opaque. In *Mtb* infected foamy
83 macrophages, bacteria containing phagosomes are found in close apposition to intracellular lipid
84 droplets (Peyron et al., 2008). It is believed that the bacterial induction of a foamy macrophage
85 phenotype in host cells results in a steady supply of lipids that addresses the bacteria's nutritional
86 requirements (Peyron et al., 2008; Russell et al., 2009; Singh et al., 2012; Daniel et al., 2011). In
87 fact, intracellular *Mtb* has been shown to import fatty acids from host lipid droplet derived

88 triacylglycerols (Daniel et al., 2011). However, other studies indicate that macrophage lipid
89 droplet formation in response to *Mtb* infection can lead to the induction of a protective, anti-
90 microbial response (Knight et al., 2018). *Mtb* appears unable to acquire host lipids when lipid
91 droplets are induced by stimulation with interferon gamma (IFN-γ) (Knight et al., 2018).
92 Moreover, there is some evidence that lipid droplets can be sites for the production of host
93 protective pro-inflammatory eicosanoids (Knight et al., 2018; Daniel et al., 2011). Lipid droplets
94 can also act as innate immune hubs against intracellular bacterial pathogens by clustering anti-
95 bacterial proteins (Bosch et al., 2020). Inhibition of macrophage fatty acid oxidation by knocking
96 out mitochondrial carnitine palmitoyl transferase 2 (CPT2) or using chemical inhibitors of CPT2
97 also restrict intracellular growth of *Mtb* (Chandra et al., 2020; Huang et al., 2018). These data
98 demonstrate that modulation of the different stages in lipid metabolism inside *Mtb* infected
99 macrophages can result in opposing outcomes.
100
101 We carried out a candidate-based, CRISPR mediated knockout of lipid import and metabolism
102 genes in macrophages to determine their roles in intracellular growth of *Mtb*. By targeting genes
103 involved in fatty acid import, sequestration, and metabolism in Hoxb8 derived conditionally
104 immortalized murine macrophages (Kiritsy et al., 2021), we show that impairing lipid homeostasis
105 in macrophages at different steps in the process negatively impacts the growth of intracellular
106 *Mtb*, albeit to differing degrees. The impact on *Mtb* growth in the mutant macrophages was
107 mediated through different mechanisms despite some common anti-microbial effectors. *Mtb*
108 infected macrophages deficient in the import of long chain fatty acids increased production of
109 pro-inflammatory markers such as interleukin 1β (IL-1β). In contrast, ablation of lipid droplet
110 biogenesis and fatty acid oxidation increased production of reactive oxygen species and limited
111 the bacteria's access to nutrients. We also found that suppression of *Mtb* growth in macrophages
112 that are unable to produce lipid droplets could not be rescued by exogeneous addition of fatty
113 acids indicating that this is not purely nutritional restriction. Our data indicate that interference
114 of lipid metabolism in macrophages leads to suppression of *Mtb* growth via multiple routes.
115
116

Results

Knockout of fatty acid import and metabolism genes restricts *Mtb* growth in macrophages

To apply a holistic approach to assessing the role(s) of fatty acid metabolism on the intracellular growth of *Mtb*, we used a CRISPR genetic approach to knockout genes involved in lipid import (CD36, FATP1), lipid droplet formation (PLIN2) and fatty acid oxidation (CPT1A, CPT2) in mouse primary macrophages (Figure 1A). Deletion of CD36 or CPT2 from mouse macrophages has been shown to impair intracellular growth of *Mtb* (Hawkes et al., 2010; Chandra et al., 2020). But the role of specialized long chain fatty acid transporters (FATP1-6) on *Mtb* growth in macrophages is uncharacterized. FATP1 and FATP4 are the most abundant fatty acid transporter isoforms in macrophages (Nishiyama et al., 2018). PLIN2, or adipophilin, is known to be required for lipid droplet formation (Paul et al., 2008; Larigauderie et al., 2004). Five isoforms of mammalian perilipins (PLIN) are involved in lipid droplet biogenesis amongst which PLIN2 is the dominant isoform expressed in macrophages (Knight et al., 2018). However, macrophages derived from PLIN2$^{-/-}$ mice show no defects in production of lipid droplets nor do they impair intracellular growth of *Mtb* (Knight et al., 2018). We targeted each of these genes with at least 2 sgRNAs in Hoxb8 Cas9^{+} conditionally immortalized myeloid progenitors (Kiritsy et al., 2021) to generate a panel of mutants that were deficient in the following candidates of interest; FATP1$^{-/-}$, PLIN2$^{-/-}$, CD36$^{-/-}$, CPT1A$^{-/-}$ and CPT2$^{-/-}$. Each individual sgRNA achieved >85% CRISPR-mediated deletion efficiency for all the 5 genes, as analyzed by the Inference for CRISPR Edits (ICE) tool (Conant et al., 2022) (Supplementary file 1). We verified the protein knockout phenotypes by flow cytometry and western blot analysis of differentiated macrophages derived from the CRISPR deleted Hoxb8 myeloid precursors (Figure 1 – figure supplement 1).

To confirm certain knockout phenotypes functionally, we checked lipid droplet biogenesis in PLIN2$^{-/-}$ macrophages in comparison to macrophages transduced with a non-targeting scramble sgRNA by confocal microscopy of BODIPY stained cells. Cells were cultured for 24 hours in the presence of exogenous oleate to enhance the formation of lipid droplets (Listenberger and Brown, 2007). We observed a complete absence of lipid droplet formation in PLIN2$^{-/-}$ macrophages as compared to controls (Figure 1 - figure supplement 2A). This is contrary to previous observations in macrophages derived from PLIN2 knockout mice which were reported

146 to have no defect in lipid droplet formation (Knight et al., 2018). We also assessed the ability of
147 CPT2$^{-/-}$ macrophages to oxidize fatty acids using the Agilent Seahorse XF Palmitate Oxidation
148 Stress Test. Scrambled sgRNA and CPT2$^{-/-}$ macrophages were cultured in substrate limiting
149 conditions and supplied with either bovine serum albumin (BSA) or BSA conjugated palmitate. As
150 shown in Figure 1 - figure supplement 2B, control macrophages were able to utilize and oxidize
151 palmitate in substrate limiting conditions indicated by a significant increase in oxygen
152 consumption rates (OCRs) in contrast to cells supplied with BSA alone. Addition of the CPT1A
153 inhibitor, etomoxir, inhibited the cell's ability to use palmitate in these conditions (Figure 1 - figure
154 supplement 2B). CPT2 knockout in CPT2$^{-/-}$ macrophages impaired the cell's ability to oxidize
155 palmitate to a degree comparable to etomoxir treatment as evidenced by baseline OCRs when
156 compared to scrambled sgRNA control (Figure 1 - figure supplement 2C).

157 We then assessed the different knockout mutant macrophages in their ability to support
158 the intracellular growth of *Mtb*. We infected macrophages with *Mtb* Erdman at a multiplicity of
159 infection (MOI) of 0.4 and assessed intracellular bacterial growth rates by counting colony forming
160 units (CFUs) 5 days post infection. All the 5 mutant macrophages significantly impaired *Mtb*
161 growth rates when compared to scrambled sgRNA as assessed by CFUs counts on day 5 (Figure
162 1B). PLIN2$^{-/-}$, FATP1$^{-/-}$ and CPT2$^{-/-}$ macrophages displayed the strongest growth restriction
163 phenotypes while CD36$^{-/-}$macrophages had a moderate, but significant, impact on *Mtb* growth.
164 In parallel, we quantified intracellular bacteria on day 0, 3 hours post infection (Figure 1C), to
165 ascertain that subsequent differences on day 5 were not due to any disparity in initial bacterial
166 uptake. The moderate growth restriction phenotypes of CD36$^{-/-}$ macrophages were consistent
167 with previous findings which reported similar impact on *Mtb* and *M. marinum* growth in
168 macrophages derived from CD36$^{-/-}$ mice (Hawkes et al., 2010). Impaired growth of *Mtb* in CPT1A^{-}
169 $^{/-}$ and CPT2$^{-/-}$ macrophages is also consistent with previous reports that genetic and chemical
170 inhibition of fatty acid oxidation is detrimental to the growth of *Mtb* within macrophages (Huang
171 et al., 2018; Chandra et al., 2020).
172
173

174 ***Mtb* infected macrophages with impaired fatty acid import and metabolism display altered**
175 **mitochondrial metabolism and elevated glycolysis.**
176 Impairment of fatty acids metabolism by FATP1 knockout in macrophages rewires their substrate
177 bias from fatty acids to glucose (Johnson et al., 2016). We reasoned that deletion of genes
178 required for downstream processing of lipids (Figure 1A) could also reprogram macrophages and
179 increase glycolysis which could, in part, explain bacterial growth restriction. We analyzed the
180 metabolic states of 3 knockout macrophages (FATP1$^{-/-}$, PLIN2$^{-/-}$ and CPT2$^{-/-}$) in uninfected and *Mtb*
181 infected conditions by monitoring oxygen consumption rates (OCR) and extracellular acidification
182 rates (ECARs) using the Agilent Mito and Glucose Stress Test kits. All 3 mutant uninfected
183 macrophages displayed reduced mitochondrial respiration as evidenced by lower basal and spare
184 respiratory capacity (SRC) when compared to scrambled sgRNA controls (Figure 2 - figure
185 supplement 1A, 1B). *Mtb* infection proportionally reduced basal and SRC rates across all the
186 mutant macrophages and scrambled controls (Figure 2A, 2B) when compared to uninfected
187 macrophages, which is consistent with previous findings (Cumming et al., 2018). PLIN2$^{-/-}$
188 macrophages displayed the most marked reduction in mitochondrial activity in both uninfected
189 and infected conditions, while FATP1$^{-/-}$ macrophages were the least affected (Figure 2A, Figure 2
190 - figure supplement 1A). As reported previously (Johnson et al., 2016), uninfected FATP1$^{-/-}$
191 macrophages were more glycolytically active with higher basal and spare glycolytic capacity (SGC)
192 compared to scrambled controls (Figure 2 - figure supplement 1C, 1D). Uninfected PLIN2$^{-/-}$ and
193 CPT2$^{-/-}$ macrophages were also more glycolytically active, but to a greater degree than FATP1$^{-/-}$
194 (Figure 2 - figure supplement 1C, 1D). *Mtb* infection increased the glycolytic capacity of all the 3
195 mutant macrophages (Figure 2C, 2D). Overall, PLIN2$^{-/-}$ macrophages exhibited the highest
196 glycolytic capacity (Figure 2C, Figure 2 - figure supplement 1D). Our data indicates that
197 impairment of fatty acid metabolism at different steps significantly impacts mitochondrial
198 respiration and reprograms cells towards glycolysis. Increased glycolytic flux in macrophages has
199 been linked to the control of intracellular *Mtb* growth (Gleeson et al., 2016; Shi et al., 2015).
200 Metabolic realignment as a consequence of interference with lipid homeostasis, which results in
201 enhanced glycolysis may contribute to *Mtb* growth restriction in these mutant macrophages.
202

203 **Knockout of lipid import and metabolism genes in macrophages activates AMPK and stabilizes**
204 **HIF-1α**
205 *Mtb* infection is known to induce increased glycolysis or the "Warburg effect" in macrophages,
206 mouse lungs and human TB granulomas (Shi et al., 2015; Gleeson et al., 2016; Belton et al., 2016).
207 Several studies have demonstrated that the Warburg effect is mediated by the master
208 transcription factor hypoxia-inducible factor-1 (HIF-1) (Courtnay et al., 2015). During *Mtb*
209 infection, HIF-1 is activated by production of reactive oxygen species (ROS), TCA cycle
210 intermediates and hypoxia in the cellular microenvironments as a consequence of altered
211 metabolic activities and increased immune cell functions (Li et al., 2024; Shi et al., 2015; Gleeson
212 et al., 2016; Belton et al., 2016). We assessed HIF-1 stability in the 3 mutant macrophage lineages
213 (FATP1$^{-/-}$, PLIN2$^{-/-}$ and CPT2$^{-/-}$) by monitoring total HIF-1α protein levels by western blot, having
214 confirmed that they were all more glycolytically active than the scrambled controls (Figure 2,
215 Figure 2 - figure supplement 1). Indeed, all the 3 mutant macrophages displayed significantly
216 higher amounts of total HIF-1α when compared to scrambled controls in uninfected conditions
217 and after *Mtb* infection for 48 hours (Figure 3A, 3B). We also checked the phosphorylation status
218 of the adenosine monophosphate kinase (AMPK), a master regulator of cell energy homeostasis
219 (Garcia and Shaw, 2017), in the mutant macrophages since Seahorse flux analyses indicated that
220 they had impaired mitochondrial activities (Figure 2, Figure 2 - figure supplement 1). Western blot
221 analysis revealed that in both *Mtb* infected and uninfected conditions, impaired fatty acid
222 metabolism correlated with moderate activation of AMPK as indicated by increased AMPK
223 phosphorylation (Figure 3C, 3D). These data point to a metabolic reprogramming of cells through
224 activation of HIF-1α and AMPK to promote glycolysis. In energetically stressed cellular
225 environments, activated AMPK promotes catabolic processes such as autophagy to maintain
226 nutrient supply and energy homeostasis (Garcia and Shaw, 2017). Autophagy is also an innate
227 immune defense mechanism against intracellular *Mtb* in macrophages (Gutierrez et al., 2004).
228 We examined the levels of autophagic flux in the mutant macrophages by monitoring LC3I to LC3II
229 conversion by western blot and by qPCR analysis of selected autophagy genes (*AMBRA1*, *ATG7*,
230 *MAP1LC3B* and *ULK1)*. We observed a moderate increase in autophagic flux by western blot in
231 uninfected FATP1$^{-/-}$ and CPT2$^{-/-}$ macrophages, which was amplified upon infection with *Mtb*

232 (Figure 2 - figure supplement 2A, 2B). Our qPCR analysis revealed that the 4 autophagy genes
233 were upregulated in both *Mtb* infected and uninfected conditions in all the 3 mutants (Figure 2 -
234 figure supplement 2C, 2D). These data suggest that impaired fatty acid import and metabolism in
235 macrophages could be restricting *Mtb* growth by promoting autophagy. These data agree with
236 previous observations that inhibition of fatty acid oxidation enhances macrophage xenophagic
237 activity whichleads to improved control of *Mtb* (Chandra et al., 2020).
238
239 **Exogenous oleate fails to rescue the *Mtb icl1*-deficient mutant in FATP1$^{-/-}$, PLIN2$^{-/-}$ and CPT2$^{-/-}$**
240 **macrophages**
241 The mycobacterial isocitrate lyase (*icl1*) acts as an isocitrate lyase in the glyoxylate shunt and as a
242 methyl-isocitrate lyase in the methyl-citrate cycle (MCC) (Gould et al., 2006; McKinney et al.,
243 2000). *Mtb* uses the MCC to convert propionyl CoA originating from the breakdown of cholesterol
244 rings and β-oxidation of odd chain fatty acids into succinate and pyruvate, which are eventually
245 assimilated into the TCA cycle (Muñoz-Elías et al., 2006; Griffin et al., 2012). The buildup of
246 propionyl CoA is toxic to *Mtb* and the bacteria relies on the MCC together with the incorporation
247 of propionyl CoA to methyl-branched lipids in the cell wall as an internal detoxification system
248 (Muñoz-Elías et al., 2006; Savvi et al., 2008). *Mtb* propionyl CoA toxicity is, in part, due to a cellular
249 imbalance between propionyl CoA and acetyl CoA as an accumulation of the former or paucity of
250 the latter results in the propionyl CoA mediated inhibition of pyruvate dehydrogenase (Lee et al.,
251 2013). Consequently, *Mtb icl1* deficient mutants (*Mtb ⊿icl1*) are unable to grow in media
252 supplemented with cholesterol or propionate, or intracellularly in macrophages (Lee et al., 2013).
253 However, this growth inhibition could be rescued both in culture and in macrophages by
254 exogenous supply of acetate or even chain fatty acids which can be oxidized to acetyl-CoA (Lee et
255 al., 2013). We took advantage of this metabolic knowledge to assess whether exogenous addition
256 of the even chain fatty acid oleate can rescue the intracellular growth of *Mtb ⊿icl1* mutants in our
257 CRISPR knockout macrophages. Scrambled controls, FATP1$^{-/-}$, PLIN2$^{-/-}$ and CPT2$^{-/-}$ macrophages in
258 normal macrophage media or media supplemented with oleate were infected with an *Mtb ⊿icl1*
259 strain expressing mCherry at MOI 5. Bacterial growth measured by mCherry expression was
260 recorded 5 days post infection. Consistent with previous observations (Lee et al., 2013), the *Mtb*

261 *Δicl1* mutant failed to replicate in both mutant and scramble macrophages that were grown in
262 normal macrophage media as evidenced by baseline mCherry fluorescence (Figure 4A). Oleate
263 supplementation successfully rescued the *Mtb Δicl1* mutant in scrambled control macrophages.
264 However, the growth restriction of the *Mtb Δicl1* strain could not be alleviated by exogenous
265 addition of oleate to the mutant macrophages (FATP1$^{-/-}$, PLIN2$^{-/-}$ and CPT2$^{-/-}$) (Figure 4A). These
266 data suggest that impaired import (FATP1$^{-/-}$), sequestration (PLIN2$^{-/-}$) or β-oxidation of fatty acids
267 (CPT2$^{-/-}$) blocks *Mtb*'s ability to access and use cellular lipids.
268 Oleate supplementation in macrophages induces the formation of lipid droplets and we
269 were able to confirm the inability to produce lipid droplets in PLIN2$^{-/-}$ macrophages using this
270 approach (Figure 1 - figure supplement 2A). As an indirect measure to track the fate of
271 supplemented oleate in the mutant macrophages, we monitored lipid droplet biogenesis in
272 FATP1$^{-/-}$ and CPT2$^{-/-}$ macrophages to check if the inability to rescue the *Mtb Δicl1* impaired growth
273 phenotypes in these mutant macrophages could be possibly related to disruptions in lipid droplet
274 biogenesis. Confocal analysis of BODIPY stained cells upon oleate supplementation revealed that
275 FATP1$^{-/-}$ macrophages also fail to generate lipid droplets (Figure 4B). In contrast, CPT2$^{-/-}$
276 macrophages produced more and larger lipid droplets in comparison to scrambled controls
277 (Figure 4B). These data suggest that the inhibition of *Mtb* growth in these mutant macrophages
278 is not merely through limitation of access to fatty acid nutrients.
279
280 **Dual RNA sequencing to identify host and bacterial determinants of *Mtb* restriction in mutant**
281 **macrophage lineages.**
282 We performed RNA sequencing of both host and bacteria in *Mtb* infected mutant macrophages
283 as a preliminary step in identification of pathways restricting bacterial growth. We infected
284 scrambled controls, FATP1$^{-/-}$, PLIN2$^{-/-}$ and CPT2$^{-/-}$ macrophages with the *Mtb* smyc'::mCherry
285 strain for 4 days and processed the samples for dual RNA sequencing as previously described
286 (Simwela et al., 2024). Principal component analysis (PCA) of host transcriptomes revealed a
287 clustering of all the 3 mutant macrophages away from scrambled controls (Figure 5A).
288 Interestingly, there was a separation in transcriptional responses between the 3 mutant
289 macrophages as CPT2$^{-/-}$ and PLIN2$^{-/-}$ macrophages clustered closer together and more distant

290 from FATP1$^{-/-}$ (Figure 5A). Overall, using an adjusted p-value < 0.05 and absolute log2 fold change
291 > 1.2, we identified 900 genes which were differentially expressed (DE) in PLIN2$^{-/-}$ macrophages
292 (589 up, 311 down), 817 genes which were DE in FATP1$^{-/-}$ macrophages (501 up, 315 down) and
293 189 genes which were DE in CPT2$^{-/-}$ (124 up, 65 down) (Supplementary file 2, Figure 5B).
294 Consistent with the PCA analysis, Venn diagram of the DE genes (Figure 5B) indicated divergent
295 responses in the 3 mutant macrophage populations. We performed pathway enrichment analysis
296 (Wu et al., 2021) of the DE genes to identify anti-microbial pathway candidates in the 3 mutant
297 macrophages. We found that defects in fatty acid uptake in FATP1$^{-/-}$ infected macrophages
298 upregulated pro-inflammatory pathways involved in MAPK and ERK signaling and production of
299 inflammatory cytokines (IFN-γ, interleukin-6, Interleukin-1α, β) (Figure 5D, Supplementary file 3).
300 The pro-inflammatory signatures of the FATP1$^{-/-}$ macrophages are consistent with previous
301 observations that demonstrated that a deficiency in FATP1 exacerbated macrophage activation *in*
302 *vitro* and *in vivo* (Johnson et al., 2016). FATP1 is a solute carrier family member (SLC27A1) and
303 *Mtb* infected FATP1$^{-/-}$ macrophages showed reduced expression of other solute carrier
304 transporters (SLC) such as FATP4 (SLC27A4), GLUT1 (SLC2A1) and 8 SLC amino acid transporters
305 (Figure 5 - figure supplement 1A, 1B, 2A, Supplementary file 2). Interestingly, *Mtb* infected FATP1^{-}
306 $^{/-}$ macrophage transcriptomes exhibited upregulation of macrophage scavenger receptors (MSR1)
307 and the ATP binding cassette transporter ABCC1 (Figure 5 - figure supplement 1A), both of which
308 can independently transport fatty acids into cells (Vogel et al., 2022; Raggers et al., 1999).
309 Meanwhile, inability generate lipid droplets in *Mtb* infected PLIN2$^{-/-}$ macrophages led to
310 upregulation in pathways involved in ribosomal biology, MHC class 1 antigen presentation,
311 canonical glycolysis, ATP metabolic processes and type 1 interferon responses (Figure 5C,
312 Supplementary file 3). In the downregulated PLIN2$^{-/-}$ DE gene set, enriched pathways included
313 those involved in production of pro-inflammatory cytokines; interleukin-6 and 8, IFN-γ and
314 interleukin-1 (Figure 5 - figure supplement 2B, Supplementary file 3). Oxidative phosphorylation
315 and processes involved in the respiratory chain electron transport were also significantly enriched
316 in PLIN2$^{-/-}$ downregulated genes. This suggests that *Mtb* infected PLIN2$^{-/-}$ macrophages increase
317 glycolytic flux and decrease mitochondrial activities, which is consistent with our metabolic flux

318 analysis data (Figure 2). Unlike FATP1$^{-/-}$ macrophages, PLIN2$^{-/-}$ macrophages are, however, broadly
319 anti-inflammatory as most pro-inflammatory genes were downregulated upon *Mtb* infection.
320 Further downstream in the lipid processing steps, inhibition of fatty acid oxidation in CPT2^{-}
321 $^{/-}$ macrophages upregulated pathways involved in MHC class 1 antigen presentation, response to
322 IFN-γ and interleukin-1 and T-cell mediated immunity (Figure 5 - figure supplement 3,
323 Supplementary file 3). There was a limited overlap in enriched pathways in the upregulated genes
324 between *Mtb* infected CPT2$^{-/-}$ and FATP1$^{-/-}$ macrophages such as those involved in the cellular
325 responses to interleukin-1 and IFN-γ. However, many pathways over-represented in CPT2$^{-/-}$
326 macrophages were common to PLIN2$^{-/-}$ macrophages (Figure 5C, Figure 5 - figure supplement 3,
327 Supplementary file 3). Similarly, both *Mtb*-infected PLIN2$^{-/-}$ *and* CPT2$^{-/-}$ macrophages were
328 downregulated in expression of genes involved in oxidative phosphorylation (Supplementary file
329 3). We confirmed expression levels of key genes by qPCR analysis of IL-1β and the type 1
330 interferon (IFN-β) response during the early time points of infection. Indeed, 4 hours post
331 infection, IL-1β and IFN-β were both upregulated in FATP1$^{-/-}$ macrophages as compared to
332 scrambled controls consistent with their pro-inflammatory phenotype (Figure 5 - figure
333 supplement 4A, 4B). On the contrary, PLIN2$^{-/-}$ macrophages downregulated IL-1β (Figure 5 - figure
334 supplement 4B). These data indicate that macrophages respond quite divergently to the deletion
335 of the different steps in fatty acid uptake, which implies that the intracellular pressures to which
336 *Mtb* is exposed may also differ.
337
338 **Oxidative stress and nutrient limitation are major stresses experienced by *Mtb* in PLIN2$^{-/-}$ and**
339 **CPT2$^{-/-}$ macrophages**
340 We also analyzed transcriptomes from intracellular *Mtb* from scrambled controls, FATP1$^{-/-}$, CPT2^{-}
341 $^{/-}$ and PLIN2$^{-/-}$ macrophages in parallel with host transcriptomes in Figure 5A. Using an adjusted
342 p-value of < 0.1 and an absolute log2 fold change > 1.4, 0 genes were DE in FATP1$^{-/-}$ macrophages,
343 105 *Mtb* genes were DE in PLIN2$^{-/-}$ macrophages (69 up, 36 down) and 10 genes were DE in CPT2^{-}
344 $^{/-}$ macrophages (3 up, 7 down) (Figure 6A). Despite being restrictive to *Mtb* growth (Figure 1B)
345 and appearing more pro-inflammatory (Figure 5D), FATP1$^{-/-}$ macrophages did not elicit a
346 detectable shift in the transcriptional response in *Mtb,* compared to control host cells. We

347 speculate that pro-inflammatory responses in FATP1$^{-/-}$ macrophages could be enough to restrict
348 the growth of bacteria, but the resulting compensatory responses as evidenced by the
349 upregulation of macrophage scavenger receptors (Figure 5 - figure supplement 1A) alleviate some
350 of the stresses that a lack of fatty acid import could be duly exerting on the bacteria. PLIN2$^{-/-}$
351 macrophages appeared to elicit the strongest transcriptional response from *Mtb* which is
352 consistent with our CFU data (Figure 1B) as PLIN2$^{-/-}$ macrophages exhibited the strongest growth
353 restriction. Among the DE genes in *Mtb* from PLIN2$^{-/-}$ macrophages, a significant number of
354 upregulated genes are involved in nutrient assimilation (Figure 6B). *Mtb* in PLIN2$^{-/-}$ macrophages
355 upregulated CobU (Rv0254c) which is predicted to be involved in the bacteria's cobalamin
356 (Vitamin B_{12}) biosynthesis. Vitamin B_{12} is an important cofactor for the activity of *Mtb* genes
357 required for cholesterol and fatty acid utilization (Campos-Pardos et al., 2024; Savvi et al., 2008).
358 Genes involved in de novo long chain fatty acid synthesis (AccE5, Rv281) (Bazet Lyonnet et al.,
359 2014), cholesterol breakdown (HsaD, Rv3569c) (Lack et al., 2010), β-oxidation of fatty acids
360 (EchA18, Rv3373; FadE22, Rv3061c) (Schnappinger et al., 2003), purine salvage (Apt, Rv2584c)
361 (Warner et al., 2014) and tryptophan metabolism (Lott, 2020) were also upregulated in *Mtb* from
362 PLIN2$^{-/-}$ macrophages (Figure 6B). This metabolic re-alignment response is seen most frequently
363 under nutrient limiting conditions (Huang et al., 2018; Pisu et al., 2020; Theriault et al., 2022).
364 *Mtb* in PLIN2$^{-/-}$ macrophages also appears to experience a significant level of other cellular
365 stresses as genes involved in DNA synthesis and repair, general response to oxidative stress and
366 PH survival in the phagosome (DnaN, Rv0002; RecF, Rv0003; DinF, Rv2836c; Rv3242c, Rv1264)
367 were upregulated (Figure 6B). Amongst the down-regulated genes in *Mtb* in PLIN2$^{-/-}$
368 macrophages, FurA (Rv1909c), a KatG repressor was the most significant (Figure 6B,
369 Supplementary file 4). FurA downregulation derepresses the catalase peroxidase, KatG, which
370 promotes *Mtb* survival in oxidative stress conditions (Zahrt et al., 2001). These data suggest that
371 PLIN2$^{-/-}$ macrophages could be, in part, restricting *Mtb* growth by increasing production of ROS.
372 The data also suggest that, contrary to a previous report (Knight et al., 2018), blocking lipid
373 droplet formation in host macrophages does place increased nutritional and oxidative stress on
374 intracellular *Mtb*.

375 CPT2$^{-/-}$ macrophages elicited a modest shift in transcriptional response from *Mtb*, and the
376 majority of the DE genes (8 out of 10) were also DE in PLIN2$^{-/-}$ macrophages (Supplementary file
377 4). This in in agreement with the host transcription response as CPT2$^{-/-}$ and PLIN2$^{-/-}$ macrophages
378 share similar candidate anti-bacterial responses (Figure 5A-C, Figure 5 - figure supplement 3). In
379 common with the *Mtb* transcriptome response in PLIN2$^{-/-}$ macrophages, upregulated genes in
380 *Mtb* isolated from CPT2$^{-/-}$ macrophages included those involved in response to oxidative stress
381 (DinF, Rv2836c) (Supplementary file 4). To substantiate some of these pathways, we assessed the
382 levels of total cellular ROS in FATP1$^{-/-}$, PLIN2$^{-/-}$ and CPT2$^{-/-}$ macrophages in both *Mtb* infected and
383 uninfected conditions by staining the cells with the Invitrogen CellROX dye and confocal
384 microscopy analysis of live stained cells. In both infected and uninfected conditions, all the 3
385 mutants displayed significantly elevated total cellular ROS when compared to scramble controls
386 (Fig. 6 - figure supplement 1A, 1B).
387
388 **Inhibitors of lipid metabolism block intracellular growth of *Mtb* in macrophages but not in broth**
389 **culture**
390 We next examined if pharmacological inhibitors would phenocopy the growth inhibition
391 phenotypes we observed with specific gene deletions. Compounds which modulate lipid
392 homeostasis are currently being investigated for HDT against TB, which is an area of considerable
393 interest (Kim et al., 2020). Such compounds include metformin, a widely used anti-diabetic drug
394 which activates AMPK, inhibits fatty acid synthesis and promotes β-oxidation of fatty acids
395 (Fullerton et al., 2013; Singhal et al., 2014). Chemical inhibition of fatty acid β-oxidation is already
396 known to promote macrophage control of *Mtb* (Chandra et al., 2020; Huang et al., 2018). We
397 targeted macrophage lipid homeostasis with trimetazidine (TMZ), an inhibitor of β-oxidation of
398 fatty acids, metformin, and an FATP1 inhibitor, FATP1 In (Matsufuji et al., 2013). We assessed the
399 impact of these compounds on extracellular *Mtb* cultured in broth over 9 days in the presence of
400 the inhibitors (DMSO, TMZ; 500 nM, Metformin; 2 mM, FATP1 In; 10 μM, Rifampicin; 0.5 μg/ml).
401 None of the 3 lipid metabolism inhibitors had a measurable effect on *Mtb* growth in liquid culture
402 media when compared to DMSO controls (Figure 7A). Treatment with rifampicin completely
403 blocked bacterial growth under the same conditions (Figure 7A). We next infected scrambled

404 sgRNA control macrophages with *Mtb* at MOI 0.5. Inhibitors were added to infected macrophages
405 3 hours post infection and bacterial CFUs were enumerated 4 days post treatment. Consistent
406 with previous observations (Chandra et al., 2020; Singhal et al., 2014), TMZ and metformin
407 significantly reduced bacterial loads in macrophages when compared to DMSO controls (Figure
408 7B). Similarly, FATP1 In also impacted the intracellular growth of *Mtb* (Figure 7B). The results
409 provide independent data that both genetic and chemical modulation of fatty acid metabolism at
410 different steps in the process negatively impacts intracellular growth of *Mtb*.
411
412 **Discussion**
413 It is clearly established that host derived fatty acids and cholesterol are important carbon sources
414 for *Mtb* (Wilburn et al., 2018). However, the relationship between *Mtb* and the infected host cell
415 lipid metabolism remains a subject of conjecture. In this report, we characterized the role of
416 macrophage lipid metabolism on the intracellular growth of *Mtb* by a targeted CRISPR mediated
417 knockout of host genes involved in fatty acid import, sequestration and catabolism. Macrophage
418 fatty acid uptake is mediated by the scavenger receptor CD36 and specialized long chain fatty acid
419 transporters, FATP1 and FATP4 (Deng et al., 2023). Earlier studies reported that a deficiency of
420 CD36 enhances macrophage control of *Mtb,* albeit to a modest degree (Hawkes et al., 2010).
421 Work from Hawkes et al.(Hawkes et al., 2010) indicated that the anti-microbial effectors in CD36
422 deficient macrophages were not due to bacterial uptake deficiencies, differences in the rate of
423 *Mtb* induced host cell death, production of ROS or pro-inflammatory cytokines (Hawkes et al.,
424 2010). We similarly observed a moderate *Mtb* growth restriction phenotype in our CRISPR
425 generated CD36$^{-/-}$ macrophages. However, a strong growth restriction of *Mtb* was observed when
426 we knocked out the long chain fatty acid transporter, FATP1. FATP1$^{-/-}$ macrophages displayed
427 altered metabolism characterized by stabilization of HIF-1α, activated AMPK, increased glycolysis
428 and reduced mitochondrial functions. Given that both CD36 and FATP1 perform similar functions,
429 it is expected that they should be some degree of compensation between the transporters when
430 either of the genes are deleted. Indeed, we found out that FATP1 knockout resulted in the
431 upregulation of other lipid import transporters (MSR1, ABCC1). This would be consistent with the
432 moderate anti-*Mtb* phenotypes in CD36$^{-/-}$ macrophages which could easily be compensated by

433 the presence of FATPs to alleviate the reduction in fatty acid supply experienced by intracellular
434 *Mtb*. However, the FATP1$^{-/-}$ macrophage phenotype appears to be more severe on *Mtb* and could
435 be exacerbated by an elevated pro-inflammatory response as has been reported previously both
436 *in vitro* and *in vivo* (Johnson et al., 2016).
437
438 After uptake into the cells, most fatty acids either undergo β-oxidation in the mitochondria to
439 provide energy or are esterified with glycerol phosphate to form triacylglycerols that may be
440 incorporated into lipid droplets in the endoplasmic reticulum (Deng et al., 2023). Over the last 2
441 decades, it has been believed that lipid droplets are a nutrient source for *Mtb* in macrophages
442 (Russell et al., 2009; Daniel et al., 2011; Peyron et al., 2008; Singh et al., 2012). However, recent
443 work indicates lipid droplets may serve as centers for the production of pro-inflammatory markers
444 and anti-microbial peptides (Knight et al., 2018; Bosch et al., 2020). It has also been reported that
445 bone marrow macrophages derived from PLIN2$^{-/-}$ mice did not have defects in the formation of
446 lipid droplets and supported robust intracellular *Mtb* replication (Knight et al., 2018). However,
447 our mutant macrophages with myeloid specific knockout of PLIN2 are unable to form lipid
448 droplets and are defective in supporting the growth of *Mtb*. The discrepancies with previous
449 observations (Knight et al., 2018) could be a consequence of compensatory responses to PLIN2
450 knockout in whole mice which when performed at embryonic level would allow for sufficient time
451 for the cells to recover by upregulating related PLIN isoforms. In fact, PLIN2$^{-/-}$ macrophages
452 displayed the strongest anti-*Mtb* phenotypes amongst our mutants exhibiting activated AMPK,
453 increased glycolysis and autophagy and impaired mitochondrial functions. *Mtb* isolated from
454 PLIN2$^{-/-}$ macrophages displayed signatures of severe nutrient limitation and oxidative stress
455 damage.
456 It has also been previously reported that chemical, genetic or miR33 mediated blockade
457 of fatty acid β-oxidation in macrophages induces lipid droplet formation (Chandra et al., 2020;
458 Ouimet et al., 2016) but that this enhanced lipid droplet formation does not correlate with
459 improved intracellular *Mtb* growth (Chandra et al., 2020). We observed a similar phenotype as
460 CPT2$^{-/-}$ macrophages that generated larger and more abundant lipid droplets than scrambled
461 control macrophages were still restrictive to *Mtb* growth. This implies that the presence or

462 absence of lipid droplets does not in itself indicate whether a macrophage will support or restrict
463 *Mtb* growth, and that the anti-microbial environment extends beyond simple nutrient availability.
464
465 In summary, our study shows that blocking macrophage's ability to import, sequester or
466 catabolize fatty acids chemically or by genetic knockout impairs *Mtb* intracellular growth. There
467 are shared features between potential anti-microbial effectors in macrophages which lack the
468 ability to import ($FATP^{-/-}$) or metabolize fatty acids ($PLIN2^{-/-}$, $CPT2^{-/-}$) such as increased glycolysis,
469 stabilized HIF-1α, activated AMPK, enhanced autophagy and production of ROS. However, there
470 are also intriguing points of divergence as $FATP^{-/-}$ macrophages are more pro-inflammatory while
471 $PLIN2^{-/-}$ macrophages appear to be broadly anti-inflammatory. The routes to *Mtb* growth
472 restriction in these mutant macrophages are clearly more complex than the bacteria's inability to
473 acquire nutrients. The data further emphasizes that targeting fatty acid homeostasis in
474 macrophages at different steps in the process (uptake, storage and catabolism) is worthy of
475 exploring in the development of new therapeutics against tuberculosis.
476
477 **Materials and methods**
478 All materials and methods are as described (Simwela et al., 2024) unless otherwise specified.
479
480 **Flow cytometry and western blot analysis**
481 Generation of CRISPR mutant Hoxb8 macrophages was carried out described previously (Simwela
482 et al., 2024). Antibodies used for both western blot and flow cytometry were as follows: rat anti-
483 Mouse CD36:Alexa Fluor®647 (Biorad, 10 µl/million cells), rabbit anti-PLIN2 (Proteintech, 1:1000),
484 rabbit anti-FATP1 (Affinity biosciences, 1:1000), rabbit anti-CPT1A antibody (Proteintech, 1:1000),
485 rabbit anti-CPT2 antibody (Proteintech, 1:1000), rabbit anti-HIF-1α antibody (Proteintech,
486 1:1000), rabbit anti-AMPKα(1:1000, Cell signalling Technology), rabbit anti-Phospho-
487 AMPKα(1:500, Cell signalling Technology), rabbit anti-LC3B (1:1000, Cell signalling Technology)
488 and rabbit anti-β Actin (1:1000, Cell Signalling Technology). For western blots, secondary
489 antibodies used were anti-rabbit/mouse StarBright Blue 700 (1:2500, Biorad). Blots were
490 developed and imaged as described previously (Simwela et al., 2024).

491

492 **Staining for cellular lipid droplets**

493 Macrophages monolayers in Ibidi eight-well chambers were supplemented with exogenous 400
494 µM oleate for 24 hours to induce the formation of lipid droplets (Listenberger and Brown, 2007).
495 Cells were then fixed in 4% paraformaldehyde and stained with BODIPY™ 493/503 (Invitrogen, 1
496 µg/ml) in 150 mM sodium chloride. Stained cells were mounted with media containing DAPI and
497 imaged using a Leica SP5 confocal microscope.

498

499 **Seahorse XF palmitate oxidation stress test**

500 A modified Seahorse mitochondrial stress test was used to measure macrophage's ability to
501 oxidize palmitate in substrate limiting conditions. 2 days before the assay, 1 x 10^5 cells were plated
502 in Seahorse cell culture mini plates. 1 day before the assay, macrophage media was replaced with
503 the Seahorse substrate limited growth media (DMEM without pyruvate supplemented with 0.5
504 mM glucose, 1 mM glutamine, 1% FBS and 0.5 mM L-Carnitine). On the day of the assay, substrate
505 limited media was replaced with assay media (DMEM without pyruvate supplemented with 2 mM
506 glucose and 0.5 mM L-Carnitine). In selected treatment conditions, cells were either supplied with
507 bovine serum albumin (BSA), BSA palmitate or BSA palmitate plus etomoxir (4 µM). Oxygen
508 consumption rates (OCRs) were measured using the Mito Stress Test assay conditions as
509 described previously (Simwela et al., 2024).

510

511 **Rescue of the *Mtb* ∆icl1 mutant in oleate supplemented media**

512 The *Mtb* H37Rv ∆*icl1* mutant expressing mCherry (Lee et al., 2013) was used for the rescue
513 experiments. The strain was maintained in 7H9 OADC broth as previously described (Simwela et
514 al., 2024) in the presence of Kanamycin (25 µg/ml) and hygromycin (50 µg/ml). 24 hours before
515 infection, macrophages were cultured in normal macrophage media or media supplemented with
516 400 µM oleate. Cells were then infected with the *Mtb* ∆*icl1* mutant at MOI 5. The bacterial
517 mCherry signal was measured on day 0 and day 5 post infection on an Envision plate reader
518 (PerkinElmer). Oleate was maintained throughout the experiment in the rescue assay conditions.

519

520 **Measurement of total cellular ROS**

521 Uninfected or *Mtb* infected macrophages monolayers in Ibidi eight-well chambers were stained
522 with the CellROX Deep Red dye (Invitrogen) as per manufacturer's staining protocol. Live stained
523 cells were imaged on a Leica SP5 confocal microscope. Z-stacks were re-constructed in ImageJ
524 from which mean fluorescence intensities (MFI) for individual cells were obtained.

525

526 **Datasets**

527 The RNA-seq data from the Dual RNA-seq analysis of infected mouse macrophages,542
528 which includes both macrophage and *Mtb* reads are available in GEO: GSE270571

529

530 **Acknowledgements**

531 We would like to thank Dr. Jen K. Grenier and Ann E. Tate from the Cornell BRC Transcriptional
532 Regulation and Expression Facility for their help with the development of dual RNA-Seq protocols.
533 This work was supported by grants from the National Institutes of Health (AI155319, AI162598,
534 and OD032135), Bill and Melinda Gates Foundation and the Mueller Health Foundation to D.G.R.
535 EJ was supported by T32AI007349.

536

537 **References**

538

539 Almeida, P. E., Silva, A. R., Maya-Monteiro, C. M., Töröcsik, D., D'avila, H., Dezsö, B., et al. 2009.
540 *Mycobacterium bovis* bacillus Calmette-Guérin infection induces TLR2-dependent peroxisome
541 proliferator-activated receptor gamma expression and activation: functions in inflammation, lipid
542 metabolism, and pathogenesis. J Immunol*,* **183,** 1337-1345.

543 Bazet Lyonnet, B., Diacovich, L., Cabruja, M., Bardou, F., Quémard, A., Gago, G. & Gramajo, H.
544 2014. Pleiotropic effect of AccD5 and AccE5 depletion in acyl-coenzyme A carboxylase activity
545 and in lipid biosynthesis in Mycobacteria. PLoS One*,* **9,** e99853.

546 Belton, M., Brilha, S., Manavaki, R., Mauri, F., Nijran, K., Hong, Y. T., et al. 2016. Hypoxia and tissue
547 destruction in pulmonary TB. Thorax*,* **71,** 1145-1153.

548 Bosch, M., Sánchez-Álvarez, M., Fajardo, A., Kapetanovic, R., Steiner, B., Dutra, F., et al. 2020.
549 Mammalian lipid droplets are innate immune hubs integrating cell metabolism and host defense.
550 Science*,* **370**, eaay8085

551 Brzostek, A., Pawelczyk, J., Rumijowska-Galewicz, A., Dziadek, B. & Dziadek, J. 2009.
552 *Mycobacterium tuberculosis* is able to accumulate and utilize cholesterol. J Bacteriol*,* **191,** 6584-
553 6591.

554 Campos-Pardos, E., Uranga, S., Picó, A., Gómez, A. B. & Gonzalo-Asensio, J. 2024. Dependency on
555 host Vitamin B12 has shaped *Mycobacterium tuberculosis* Complex evolution. Nat Commun*,* **15,**
556 2161.

557 Chandra, P., He, L., Zimmerman, M., Yang, G., Köster, S., Ouimet, M., et al. 2020. Inhibition of fatty
558 acid oxidation promotes macrophage control of *Mycobacterium tuberculosis*. mBio*,* **11**, e01139-
559 20

560 Cohen, S. B., Gern, B. H., Delahaye, J. L., Adams, K. N., Plumlee, C. R., Winkler, J. K., et al. 2018.
561 Alveolar macrophages provide an early *Mycobacterium tuberculosis* niche and initiate
562 dissemination. Cell Host Microbe*,* **24,** 439-446.e4.

563 Conant, D., Hsiau, T., Rossi, N., Oki, J., Maures, T., Waite, K., et al. 2022. Inference of CRISPR edits
564 from Sanger trace data. CRISPR J*,* **5,** 123-130.

565 Courtnay, R., Ngo, D. C., Malik, N., Ververis, K., Tortorella, S. M. & Karagiannis, T. C. 2015. Cancer
566 metabolism and the Warburg effect: the role of HIF-1 and PI3K. Mol Biol Rep*,* **42,** 841-851.

567 Cumming, B. M., Addicott, K. W., Adamson, J. H. & Steyn, A. J. 2018. *Mycobacterium tuberculosis*
568 induces decelerated bioenergetic metabolism in human macrophages. Elife*,* **7**, e39169

569 Daniel, J., Maamar, H., Deb, C., Sirakova, T. D. & Kolattukudy, P. E. 2011. *Mycobacterium*
570 *tuberculosis* uses host triacylglycerol to accumulate lipid droplets and acquires a dormancy-like
571 phenotype in lipid-loaded macrophages. PLoS Pathog*,* **7,** e1002093.

572 Deng, L., Kersten, S. & Stienstra, R. 2023. Triacylglycerol uptake and handling by macrophages:
573 from fatty acids to lipoproteins. Progress in Lipid Research, **92,** 101250.

574 Fullerton, M. D., Galic, S., Marcinko, K., Sikkema, S., Pulinilkunnil, T., Chen, Z. P., et al. 2013. Single
575 phosphorylation sites in ACC1 and ACC2 regulate lipid homeostasis and the insulin-sensitizing
576 effects of metformin. Nat Med, **19,** 1649-1654.

577 Garcia, D. & Shaw, R. J. 2017. AMPK: mechanisms of cellular energy sensing and restoration of
578 metabolic balance. Mol Cell, **66,** 789-800.

579 Gleeson, L. E., Sheedy, F. J., Palsson-Mcdermott, E. M., Triglia, D., O'leary, S. M., O'sullivan, M. P.,
580 et al. 2016. Cutting edge: *Mycobacterium tuberculosis* induces aerobic glycolysis in human
581 alveolar macrophages that is required for control of intracellular bacillary replication. J Immunol,
582 **196,** 2444-2449.

583 Gould, T. A., Van De Langemheen, H., Muñoz-Elías, E. J., Mckinney, J. D. & Sacchettini, J. C. 2006.
584 Dual role of isocitrate lyase 1 in the glyoxylate and methylcitrate cycles in *Mycobacterium*
585 *tuberculosis*. Mol Microbiol, **61,** 940-947.

586 Griffin, J. E., Pandey, A. K., Gilmore, S. A., Mizrahi, V., Mckinney, J. D., Bertozzi, C. R. & Sassetti, C.
587 M. 2012. Cholesterol catabolism by *Mycobacterium tuberculosis* requires transcriptional and
588 metabolic adaptations. Chem Biol, **19,** 218-227.

589 Gutierrez, M. G., Master, S. S., Singh, S. B., Taylor, G. A., Colombo, M. I. & Deretic, V. 2004.
590 Autophagy is a defense mechanism inhibiting BCG and *Mycobacterium tuberculosis* survival in
591 infected macrophages. Cell, **119,** 753-766.

592 Hawkes, M., Li, X., Crockett, M., Diassiti, A., Finney, C., Min-Oo, G., et al. 2010. CD36 deficiency
593 attenuates experimental Mycobacterial infection. BMC Infect Dis, **10,** 299.

594 Huang, L., Nazarova, E. V., Tan, S., Liu, Y. & Russell, D. G. 2018. Growth of *Mycobacterium*
595 *tuberculosis* in vivo segregates with host macrophage metabolism and ontogeny. J Exp Med, **215,**
596 1135-1152.

597 Johnson, A. R., Qin, Y., Cozzo, A. J., Freemerman, A. J., Huang, M. J., Zhao, L., et al. 2016. Metabolic
598 reprogramming through fatty acid transport protein 1 (FATP1) regulates macrophage
599 inflammatory potential and adipose inflammation. Mol Metab*,* **5,** 506-526.

600 Kim, J. S., Kim, Y. R. & Yang, C. S. 2020. Host-directed therapy in tuberculosis: targeting host
601 metabolism. Front Immunol*,* **11,** 1790.

602 Kim, M. J., Wainwright, H. C., Locketz, M., Bekker, L. G., Walther, G. B., Dittrich, C., et al. 2010.
603 Caseation of human tuberculosis granulomas correlates with elevated host lipid metabolism.
604 EMBO Mol Med*,* **2,** 258-274.

605 Kim, Y. S., Lee, H. M., Kim, J. K., Yang, C. S., Kim, T. S., Jung, M., et al. 2017. PPAR-α Activation
606 mediates innate host defense through induction of TFEB and lipid catabolism. J Immunol*,* **198,**
607 3283-3295.

608 Kiritsy, M. C., Mccann, K., Mott, D., Holland, S. M., Behar, S. M., Sassetti, C. M. & Olive, A. J. 2021.
609 Mitochondrial respiration contributes to the interferon gamma response in antigen-presenting
610 cells. Elife*,* **10**, e65109

611 Knight, M., Braverman, J., Asfaha, K., Gronert, K. & Stanley, S. 2018. Lipid droplet formation in
612 *Mycobacterium tuberculosis* infected macrophages requires IFN-γ/HIF-1α signaling and supports
613 host defense. PLoS Pathog*,* **14,** e1006874.

614 Lack, N. A., Yam, K. C., Lowe, E. D., Horsman, G. P., Owen, R. L., Sim, E. & Eltis, L. D. 2010.
615 Characterization of a carbon-carbon hydrolase from *Mycobacterium tuberculosis* involved in
616 cholesterol metabolism. J Biol Chem*,* **285,** 434-443.

617 Larigauderie, G., Furman, C., Jaye, M., Lasselin, C., Copin, C., Fruchart, J. C., et al. 2004. Adipophilin
618 enhances lipid accumulation and prevents lipid efflux from THP-1 macrophages: potential role in
619 atherogenesis. Arterioscler Thromb Vasc Biol*,* **24,** 504-510.

620 Lee, W., Vanderven, B. C., Fahey, R. J. & Russell, D. G. 2013. Intracellular *Mycobacterium*
621 *tuberculosis* exploits host-derived fatty acids to limit metabolic stress. J Biol Chem*,* **288,** 6788-
622 6800.

623 Li, C., Wang, J., Xu, J. F., Pi, J. & Zheng, B. 2024. Roles of HIF-1α signaling in *Mycobacterium*
624 *tuberculosis* infection: new targets for anti-TB therapeutics? Biochem Biophys Res Commun*,* **711,**
625 149920.

626 Listenberger, L. L. & Brown, D. A. 2007. Fluorescent detection of lipid droplets and associated
627 proteins. Curr Protoc Cell Biol*,* **Chapter 24,** Unit 24.2.

628 Lott, J. S. 2020. The tryptophan biosynthetic pathway is essential for *Mycobacterium tuberculosis*
629 to cause disease. Biochem Soc Trans*,* **48,** 2029-2037.

630 Matsufuji, T., Ikeda, M., Naito, A., Hirouchi, M., Kanda, S., Izumi, M., et al. 2013. Arylpiperazines
631 as fatty acid transport protein 1 (FATP1) inhibitors with improved potency and pharmacokinetic
632 properties. Bioorg Med Chem Lett*,* **23,** 2560-2565.

633 Mckinney, J. D., Höner Zu Bentrup, K., Muñoz-Elías, E. J., Miczak, A., Chen, B., Chan, W. T., et al.
634 2000. Persistence of *Mycobacterium tuberculosis* in macrophages and mice requires the
635 glyoxylate shunt enzyme isocitrate lyase. Nature*,* **406,** 735-738.

636 Muñoz-Elías, E. J. & Mckinney, J. D. 2005. *Mycobacterium tuberculosis* isocitrate lyases 1 and 2
637 are jointly required for in vivo growth and virulence. Nat Med*,* **11,** 638-644.

638 Muñoz-Elías, E. J., Upton, A. M., Cherian, J. & Mckinney, J. D. 2006. Role of the methylcitrate cycle
639 in *Mycobacterium tuberculosis* metabolism, intracellular growth, and virulence. Mol Microbiol*,*
640 **60,** 1109-22.

641 Nishiyama, K., Fujita, T., Fujimoto, Y., Nakajima, H., Takeuchi, T. & Azuma, Y.-T. 2018. Fatty acid
642 transport protein 1 enhances the macrophage inflammatory response by coupling with ceramide
643 and c-Jun N-terminal kinase signaling. Int Immunopharmacol*,* **55,** 205-215.

644 Ouimet, M., Koster, S., Sakowski, E., Ramkhelawon, B., Van Solingen, C., Oldebeken, S., et al. 2016.
645 *Mycobacterium tuberculosis* induces the miR-33 locus to reprogram autophagy and host lipid
646 metabolism. Nat Immunol*,* **17,** 677-686.

647 Pandey, A. K. & Sassetti, C. M. 2008. *Mycobacterial* persistence requires the utilization of host
648 cholesterol. Proc Natl Acad Sci U S A*,* **105,** 4376-4380.

649 Parihar, S. P., Guler, R., Khutlang, R., Lang, D. M., Hurdayal, R., Mhlanga, M. M., et al. 2014. Statin
650 therapy reduces the *Mycobacterium tuberculosis* burden in human macrophages and in mice by
651 enhancing autophagy and phagosome maturation. J Infect Dis*,* **209,** 754-763.

652 Paul, A., Chang, B. H., Li, L., Yechoor, V. K. & Chan, L. 2008. Deficiency of adipose differentiation-
653 related protein impairs foam cell formation and protects against atherosclerosis. Circ Res*,* **102,**
654 1492-1501.

655 Peyron, P., Vaubourgeix, J., Poquet, Y., Levillain, F., Botanch, C., Bardou, F., et al. 2008. Foamy
656 macrophages from tuberculous patients' granulomas constitute a nutrient-rich reservoir for *M.*
657 *tuberculosis* persistence. PLoS Pathog*,* **4,** e1000204.

658 Pisu, D., Huang, L., Grenier, J. K. & Russell, D. G. 2020. Dual RNA-seq of Mtb-infected macrophages
659 in vivo reveals ontologically distinct host-pathogen interactions. Cell Rep*,* **30,** 335-350 e4.

660 Pisu, D., Huang, L., Narang, V., Theriault, M., Le-Bury, G., Lee, B., et al. 2021. Single cell analysis of
661 *M. tuberculosis* phenotype and macrophage lineages in the infected lung. J Exp Med*,* **218,**
662 e20210615

663 Podinovskaia, M., Lee, W., Caldwell, S. & Russell, D. G. 2013. Infection of macrophages with
664 *Mycobacterium tuberculosis* induces global modifications to phagosomal function. Cell Microbiol*,*
665 **15,** 843-859.

666 Raggers, R. J., Van Helvoort, A., Evers, R. & Van Meer, G. 1999. The human multidrug resistance
667 protein MRP1 translocates sphingolipid analogs across the plasma membrane. J Cell Sci*,* **112 (Pt**
668 **3),** 415-422.

669 Russell, D. G., Cardona, P. J., Kim, M. J., Allain, S. & Altare, F. 2009. Foamy macrophages and the
670 progression of the human tuberculosis granuloma. Nat Immunol, **10,** 943-948.

671 Savvi, S., Warner, D. F., Kana, B. D., Mckinney, J. D., Mizrahi, V. & Dawes, S. S. 2008. Functional
672 characterization of a Vitamin B12-dependent methylmalonyl pathway in *Mycobacterium*
673 *tuberculosis*: implications for propionate metabolism during growth on fatty acids. J Bacteriol,
674 **190,** 3886-3895.

675 Schnappinger, D., Ehrt, S., Voskuil, M. I., Liu, Y., Mangan, J. A., Monahan, I. M., et al. 2003.
676 Transcriptional adaptation of *Mycobacterium tuberculosis* within Macrophages: insights into the
677 phagosomal environment. J Exp Med, **198,** 693-704.

678 Shi, L., Salamon, H., Eugenin, E. A., Pine, R., Cooper, A. & Gennaro, M. L. 2015. Infection with
679 *Mycobacterium tuberculosis* induces the Warburg effect in mouse lungs. Sci Rep, **5,** 18176.

680 Simwela, N. V., Johnston, L., Bitar, P. P., Eleni, J., Altier, C., Sassetti, C. M. & Russell, D. G. 2024.
681 Genome-wide screen of *Mycobacterium tuberculosis* infected macrophages identified the
682 GID/CTLH complex as a determinant of intracellular bacterial growth. bioRxiv**,**
683 2024.05.06.592714.

684 Singh, V., Jamwal, S., Jain, R., Verma, P., Gokhale, R. & Rao, K. V. 2012. *Mycobacterium*
685 *tuberculosis*-driven targeted recalibration of macrophage lipid homeostasis promotes the foamy
686 phenotype. Cell Host Microbe, **12,** 669-81.

687 Singhal, A., Jie, L., Kumar, P., Hong, G. S., Leow, M. K., Paleja, B., et al. 2014. Metformin as adjunct
688 antituberculosis therapy. Sci Transl Med, **6,** 263ra159.

689 Theriault, M. E., Pisu, D., Wilburn, K. M., Lê-Bury, G., Macnamara, C. W., Michael Petrassi, H., et
690 al. 2022. Iron limitation in *M. tuberculosis* has broad impact on central carbon metabolism.
691 Commun Biol, **5,** 685.

692 Vogel, A., Brunner, J. S., Hajto, A., Sharif, O. & Schabbauer, G. 2022. Lipid scavenging
693 macrophages and inflammation. Biochim Biophys Acta Mol Cell Biol Lipids, **1867,** 159066.

694 Warner, D. F., Evans, J. C. & Mizrahi, V. 2014. Nucleotide metabolism and DNA replication.
695 Microbiol Spectr*,* **2**, MGM2-0001-2013

696 WHO, 2023. Global tuberculosis report 2023. Geneva, Switzerland World Health Organisation.

697 Wilburn, K. M., Fieweger, R. A. & Vanderven, B. C. 2018. Cholesterol and fatty acids grease the
698 wheels of *Mycobacterium tuberculosis* pathogenesis. Pathog Dis*,* **76**, fty021.

699 Wolf, A. J., Linas, B., Trevejo-Nuñez, G. J., Kincaid, E., Tamura, T., Takatsu, K. & Ernst, J. D. 2007.
700 *Mycobacterium tuberculosis* infects dendritic cells with high frequency and impairs their function
701 in vivo. J Immunol*,* **179,** 2509-2519.

702 Wu, T., Hu, E., Xu, S., Chen, M., Guo, P., Dai, Z., et al. 2021. clusterProfiler 4.0: A universal
703 enrichment tool for interpreting omics data. Innovation (Camb)*,* **2,** 100141.

704 Zahrt, T. C., Song, J., Siple, J. & Deretic, V. 2001. Mycobacterial FurA is a negative regulator of
705 catalase-peroxidase gene katG. Mol Microbiol*,* **39,** 1174-1185.
706
707
708
709
710
711
712
713
714
715
716
717
718
719
720

721 **Figure legends**

722 **Figure 1. Knockout of fatty acid import and metabolism genes restricts *Mtb* growth in**
723 **macrophages**. (A) Schematic of lipid import and metabolism genes in macrophages. Genes
724 targeted for CRISPR-Cas9 mediated knockout are highlighted in red. (B) Scramble sgRNA or
725 specific mutant macrophages were infected with the *Mtb* Erdman strain at MOI 0.4. Intracellular
726 *Mtb* growth was measured by plating and counting CFUs in lysed macrophages 5 days post
727 infection (PI). (C) CFUs from lysed macrophages were also plated on day 0, 3 hours post infection
728 to demonstrate that there were minimal differences in bacterial uptake between the mutated
729 macrophage lineages. n=6; ****, $P < 0.0001$.

730

731 **Figure 2. *Mtb* infected macrophages with impaired fatty acid import and metabolism display**
732 **reduced mitochondrial activities and are more glycolytic**. (A) Seahorse flux analyses of scramble
733 or PLIN2$^{-/-}$, FATP1$^{-/-}$ and CPT2$^{-/-}$ macrophages infected with *Mtb* Erdman strain at MOI 1 24 hours
734 post infection. Oxygen consumption rates (OCR) were measured using the Cell Mito Stress Test
735 Kit (Agilent). Oligo, oligomycin; FCCP, fluoro-carbonyl cyanide phenylhydrazone; Rot/A, rotenone
736 and antimycin A. (B) Comparison of basal respiration and spare respiratory capacity (SRC) from A.
737 SRC was calculated by subtracting the normalized maximal OCR from basal OCR. n=3 (2 technical
738 repeats per replicate); ****, $P < 0.0001$. (C) Extracellular acidification rates (ECARs) of scramble
739 or PLIN2$^{-/-}$, FATP1$^{-/-}$ and CPT2$^{-/-}$ macrophages infected with *Mtb* as in A. ECARs were measured
740 using the Agilent Seahorse Glycolysis Stress Test kit. 2DG, 2-Deoxy-D-glucose. (D) Comparison of
741 basal glycolysis and spare glycolytic capacity (SGC) in the indicated mutant macrophages. SGC was
742 calculated as SRC above. n=3 (2 technical repeats per replicate); *, $P < 0.05$, ****, $P < 0.0001$.

743

744 **Figure 3. Knockout of fatty acid import and metabolism genes in macrophages activate AMPK**
745 **and stabilizes HIF-1α.** (A) Western blot analysis of HIF-1α in uninfected and *Mtb* infected
746 scramble or PLIN2$^{-/-}$, FATP1$^{-/-}$ and CPT2$^{-/-}$ macrophages. In *Mtb* infected conditions, cells were
747 infected with the bacteria at MOI 1 for 48 hours before preparation of cell lysates. (B) Western
748 blot analysis of total and phosphorylated AMPK in uninfected and *Mtb* infected scramble or
749 PLIN2$^{-/-}$, FATP1$^{-/-}$ and CPT2$^{-/-}$ *macrophages*. Cell lysates were prepared as in A.

750

751 **Figure 4. Supplementation with exogenous oleate fails to rescue the *Mtb* Δicl1 mutant in PLIN2^{-}**
752 **$^{/-}$, FATP1$^{-/-}$ and CPT2$^{-/-}$ macrophages**. (A) Scramble or indicated mutant macrophages were
753 infected with the *Mtb* H37Rv Δicl1 mutant expressing mCherry at MOI 5. Oleate supplementation
754 (400 μM) was commenced 24 hours before infection in the treatment group, removed during *Mtb*
755 infection and re-added 3-hours post infection for the entire duration of the experiment. Growth
756 kinetics of *Mtb* were measured by monitoring mCherry fluorescence using a plate reader. n=4;
757 ****, $P < 0.0001$. (B) Uninfected scramble or FATP1$^{-/-}$ and CPT2$^{-/-}$ macrophages were
758 supplemented with 400 μM oleate for 24 hours. Cells were then fixed for 20 minutes and stained
759 for lipid droplet inclusions using the Bodipy 493/503 dye. DAPI was used as a counterstain to
760 detect nuclei.

761

762 **Figure 5. Dual RNA sequencing to identify host and bacterial determinants of *Mtb* restriction in**
763 **macrophages with fatty acid import and metabolism knockout genes**. (A) Principal component
764 analysis (PCA) of scramble or PLIN2$^{-/-}$, FATP1$^{-/-}$ and CPT2$^{-/-}$ macrophages transcriptomes infected
765 with the *Mtb* smyc'::mCherry strain at MOI 0.5 4 days post infection. (B) Venn diagram of DE gene
766 sets (Supplementary file 2) in PLIN2$^{-/-}$, FATP1$^{-/-}$ and CPT2$^{-/-}$ mutant macrophages as compared to
767 scramble showing overlapping genes. DE genes cutoff; abs ($\log_2$ fold change) > 0.3, adjusted p-
768 value < 0.05. (C-D) Tree plot of top 80 enriched gene ontology terms (biological process) in *Mtb*
769 infected PLIN2$^{-/-}$ and FATP1$^{-/-}$ upregulated genes.

770

771 **Figure 6. Nutritional and oxidative stress define the core transcriptome response of *Mtb* inside**
772 **PLIN2$^{-/-}$ macrophages.** (A) Schematic showing DE genes in *Mtb* transcriptomes isolated from
773 PLIN2$^{-/-}$, FATP1$^{-/-}$ and CPT2$^{-/-}$ macrophages in Figure 5A. (B) Heatmaps of nutritional and oxidative
774 stress DE genes in PLIN2$^{-/-}$ macrophages. Arrows show genes which are also DE in CPT2$^{-/-}$
775 macrophages in a similar trend (Supplementary file 4).

776

777 **Figure 7. Inhibitors of fatty acid transport and metabolism block intracellular growth of *Mtb* in**
778 **macrophages.** (A) Growth of *Mtb* in liquid broth in the absence of drug (DMSO) or presence of

779 metformin, FATP1 inhibitor (FATP1 In, 10 μM) and the β-oxidation of fatty acid inhibitor,
780 Trimetazidine (TMZ, 500 nM). *Mtb* Erdman was grown to log phase and diluted to OD_{600} 0.01 in
781 7H9 media in the presence of the above inhibitors. Growth kinetics were monitored by OD_{600}
782 measurements using a plate reader. Rifampicin (RIF) at 0.5 μg/ml was used as a total killing
783 control. (B) Scramble macrophages were infected with *Mtb* Erdman at MOI 0.5. Inhibitors were
784 added 3 hours post infection following which CFUs were plated 4 days post infection. n=5; **, P
785 < 0.01; ****, P < 0.0001.
786
787
788
789
790
791
792

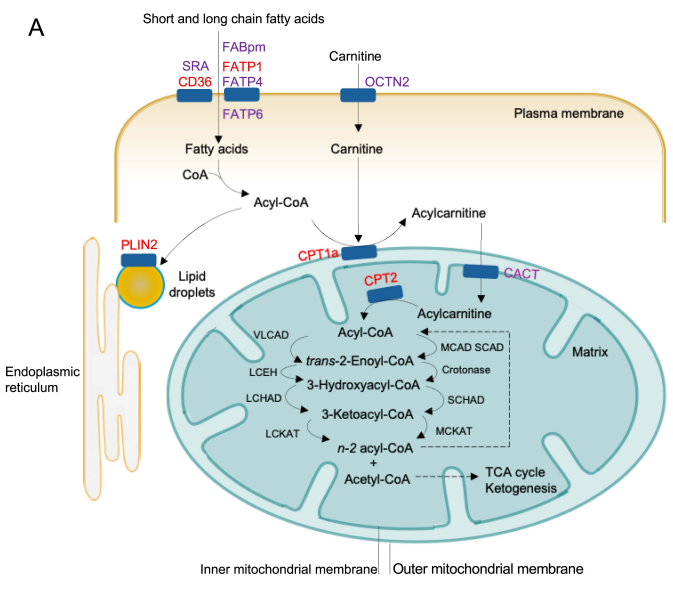
A
Short and long chain fatty acids
FABpm
SRA
CD36
FATP1
FATP4
FATP6
Carnitine
OCTN2
Plasma membrane
Fatty acids
Carnitine
CoA
Acyl-CoA
Acylcarnitine
PLIN2
Lipid droplets
CPT1a
CPT2
CACT
Acylcarnitine
Acyl-CoA
VLCAD
MCAD SCAD
trans-2-Enoyl-CoA
LCEH
Crotonase
3-Hydroxyacyl-CoA
LCHAD
SCHAD
3-Ketoacyl-CoA
LCKAT
MCKAT
n-2 acyl-CoA
+
Acetyl-CoA
TCA cycle
Ketogenesis
Matrix
Endoplasmic reticulum
Inner mitochondrial membrane
Outer mitochondrial membrane

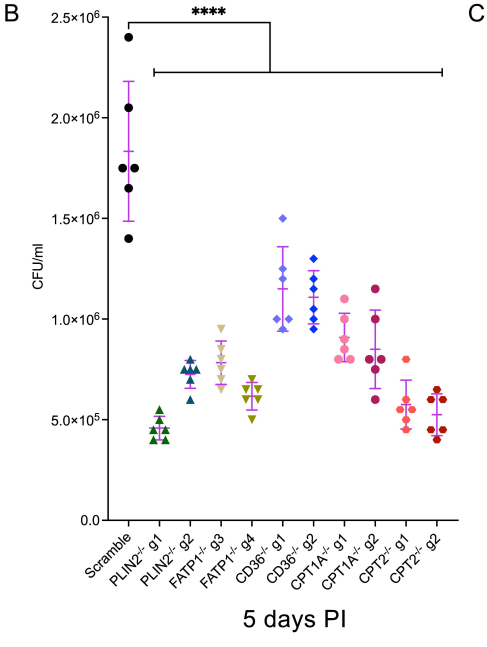
B
****
CFU/ml
2.5×10^6
2.0×10^6
1.5×10^6
1.0×10^6
5.0×10^5
0.0
Scramble
PLIN2-/- g1
PLIN2-/- g2
FATP1-/- g3
FATP1-/- g4
CD36-/- g1
CD36-/- g2
CPT1A-/- g1
CPT1A-/- g2
CPT2-/- g1
CPT2-/- g2
5 days PI

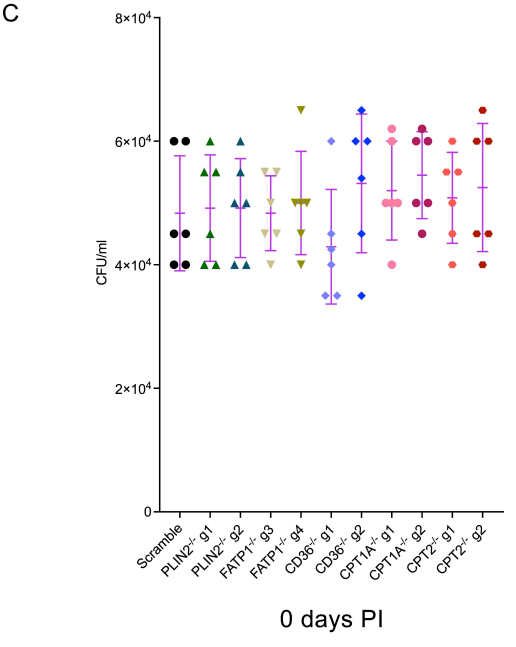
C
CFU/ml
8×10^4
6×10^4
4×10^4
2×10^4
0
Scramble
PLIN2-/- g1
PLIN2-/- g2
FATP1-/- g3
FATP1-/- g4
CD36-/- g1
CD36-/- g2
CPT1A-/- g1
CPT1A-/- g2
CPT2-/- g1
CPT2-/- g2
0 days PI

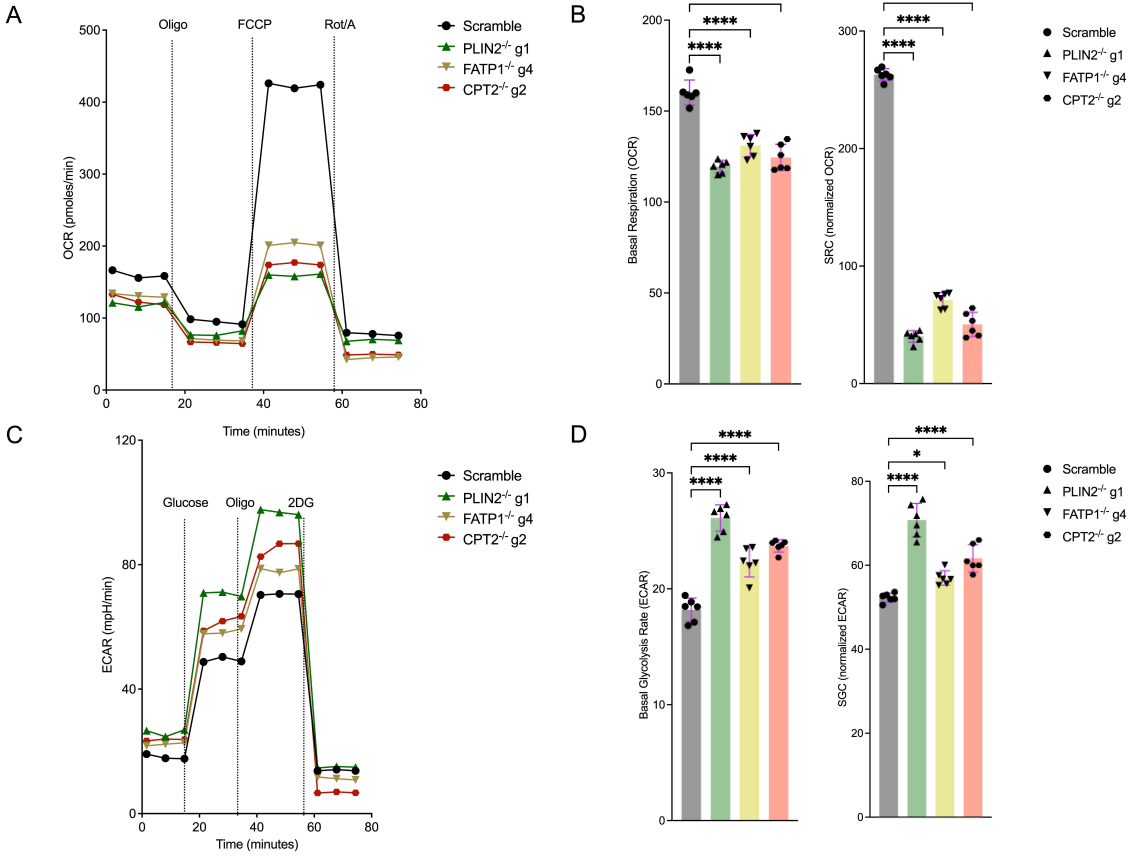
A
Oligo
FCCP
Rot/A
Scramble
PLIN2-/- g1
FATP1-/- g4
CPT2-/- g2
OCR (pmoles/min)
Time (minutes)
B
Basal Respiration (OCR)
SRC (normalized OCR)
****
C
Glucose
Oligo
2DG
ECAR (mpH/min)
D
Basal Glycolysis Rate (ECAR)
SGC (normalized ECAR)
*

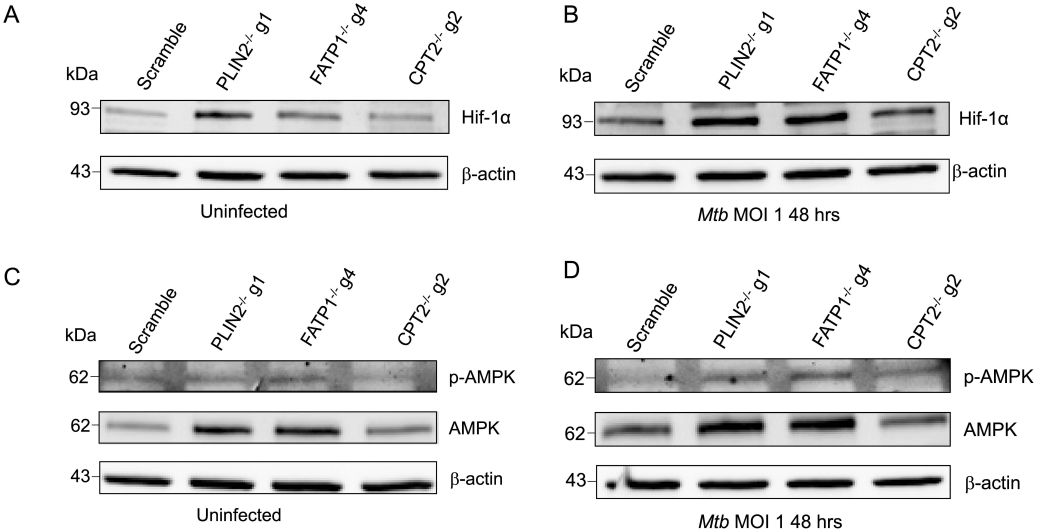
A
kDa
Scramble
PLIN2-/- g1
FATP1-/- g4
CPT2-/- g2
93
Hif-1α
43
β-actin
Uninfected
B
kDa
Scramble
PLIN2-/- g1
FATP1-/- g4
CPT2-/- g2
93
Hif-1α
43
β-actin
Mtb MOI 1 48 hrs
C
kDa
Scramble
PLIN2-/- g1
FATP1-/- g4
CPT2-/- g2
62
p-AMPK
62
AMPK
43
β-actin
Uninfected
D
kDa
Scramble
PLIN2-/- g1
FATP1-/- g4
CPT2-/- g2
62
p-AMPK
62
AMPK
43
β-actin
Mtb MOI 1 48 hrs

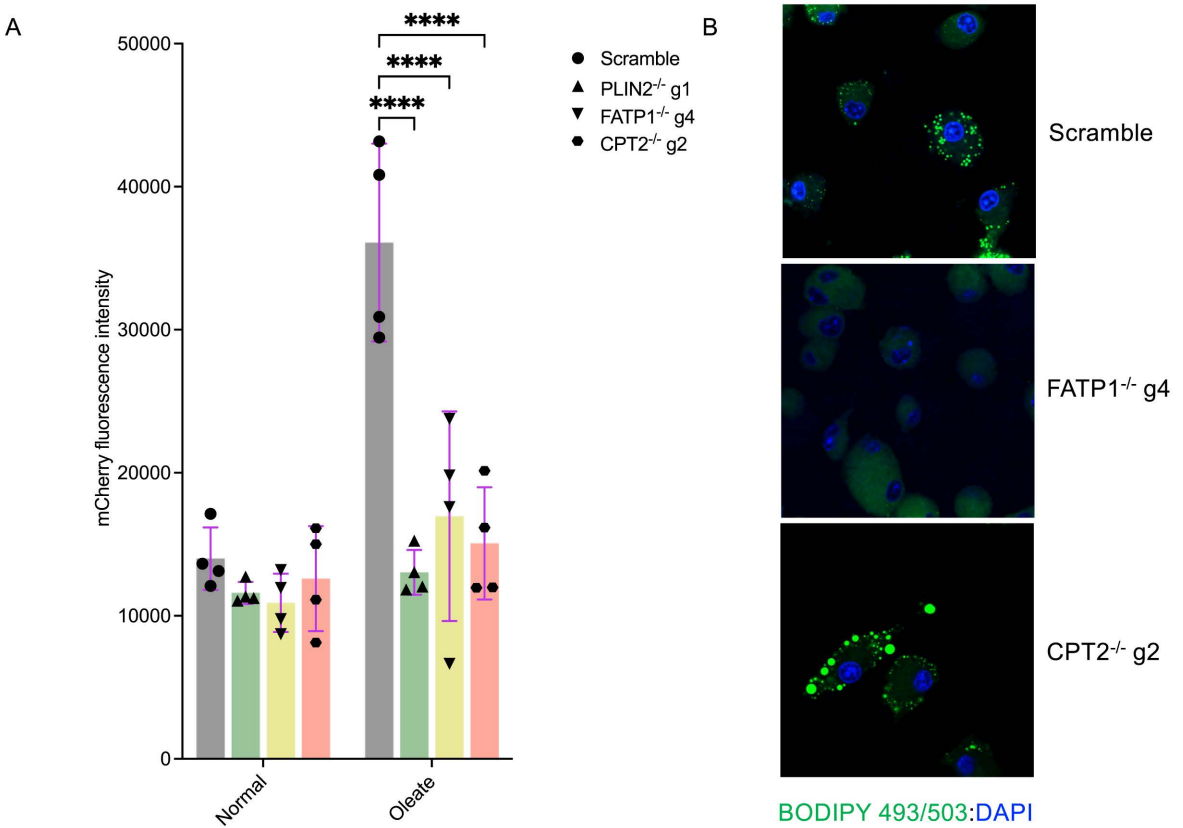
A
B
****
****
****
Scramble
PLIN2-/- g1
FATP1-/- g4
CPT2-/- g2
mCherry fluorescence intensity
50000
40000
30000
20000
10000
0
Normal
Oleate
Scramble
FATP1-/- g4
CPT2-/- g2
BODIPY 493/503:DAPI

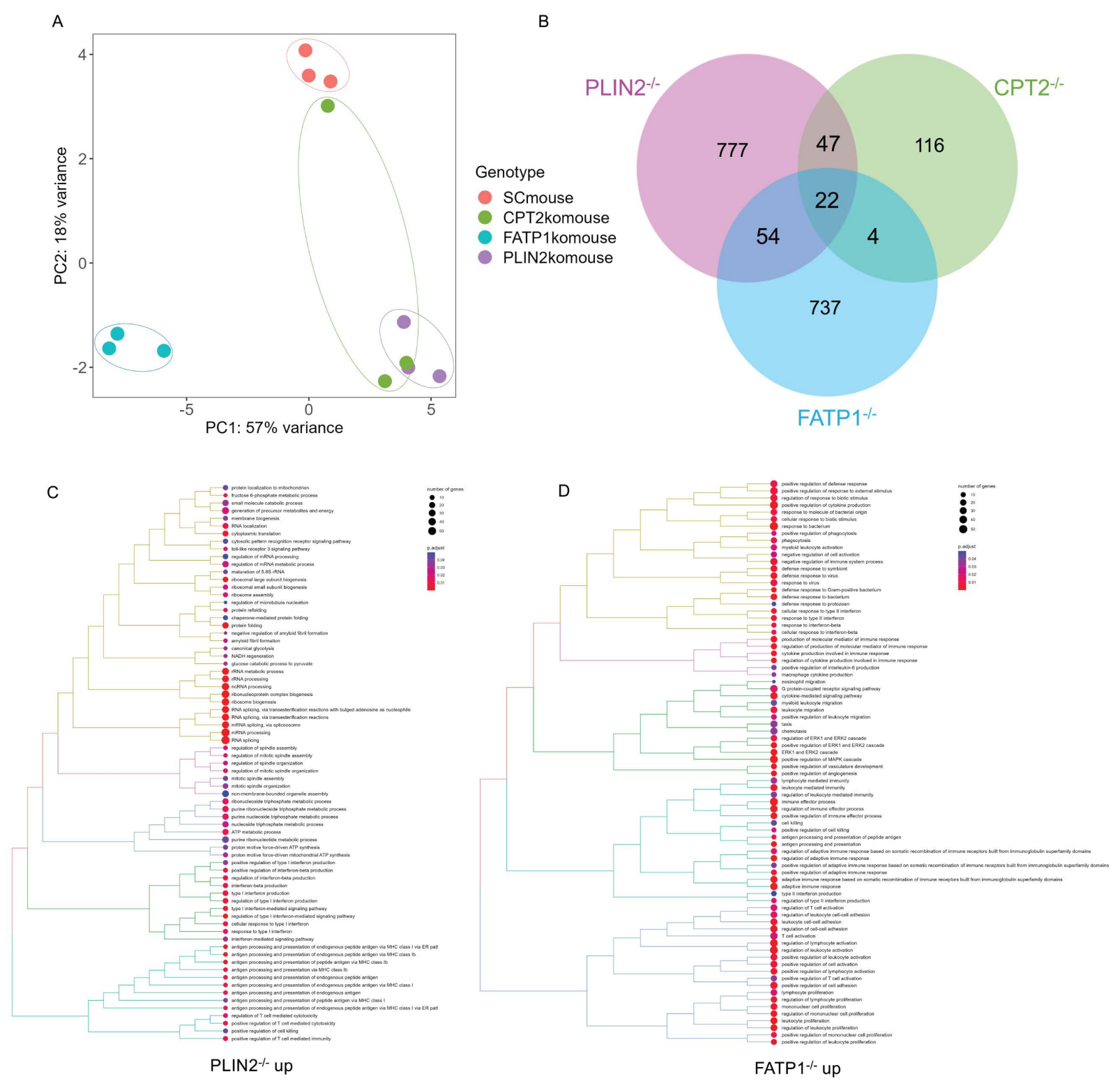
A
PC2: 18% variance
PC1: 57% variance
Genotype
SCmouse
CPT2komouse
FATP1komouse
PLIN2komouse
B
PLIN2-/-
CPT2-/-
FATP1-/-
777
47
116
22
54
4
737
C
number of genes
p.adjust
protein localization to mitochondrion
fructose 6-phosphate metabolic process
small molecule catabolic process
generation of precursor metabolites and energy
membrane biogenesis
RNA localization
cytoplasmic translation
cytosolic pattern recognition receptor signaling pathway
toll-like receptor 3 signaling pathway
regulation of mRNA processing
regulation of mRNA metabolic process
maturation of 5.8S rRNA
ribosomal large subunit biogenesis
ribosomal small subunit biogenesis
ribosome assembly
regulation of microtubule nucleation
protein refolding
chaperone-mediated protein folding
protein folding
negative regulation of amyloid fibril formation
amyloid fibril formation
canonical glycolysis
NADH regeneration
glucose catabolic process to pyruvate
rRNA metabolic process
rRNA processing
ncRNA processing
ribonucleoprotein complex biogenesis
ribosome biogenesis
RNA splicing, via transesterification reactions with bulged adenosine as nucleophile
RNA splicing, via transesterification reactions
mRNA splicing, via spliceosome
mRNA processing
RNA splicing
regulation of spindle assembly
regulation of mitotic spindle assembly
regulation of spindle organization
regulation of mitotic spindle organization
mitotic spindle assembly
mitotic spindle organization
non-membrane-bounded organelle assembly
ribonucleoside triphosphate metabolic process
purine ribonucleoside triphosphate metabolic process
purine nucleoside triphosphate metabolic process
nucleoside triphosphate metabolic process
ATP metabolic process
purine ribonucleotide metabolic process
proton motive force-driven ATP synthesis
proton motive force-driven mitochondrial ATP synthesis
positive regulation of type I interferon production
positive regulation of interferon-beta production
regulation of interferon-beta production
interferon-beta production
type I interferon production
regulation of type I interferon production
type I interferon-mediated signaling pathway
regulation of type I interferon-mediated signaling pathway
cellular response to type I interferon
response to type I interferon
interferon-mediated signaling pathway
antigen processing and presentation of endogenous peptide antigen via MHC class I via ER patl
antigen processing and presentation of endogenous peptide antigen via MHC class Ib
antigen processing and presentation of peptide antigen via MHC class Ib
antigen processing and presentation via MHC class Ib
antigen processing and presentation of endogenous peptide antigen
antigen processing and presentation of endogenous peptide antigen via MHC class I
antigen processing and presentation of endogenous antigen
antigen processing and presentation of peptide antigen via MHC class I
antigen processing and presentation of endogenous peptide antigen via MHC class I via ER patl
regulation of T cell mediated cytotoxicity
positive regulation of T cell mediated cytotoxicity
positive regulation of cell killing
positive regulation of T cell mediated immunity
PLIN2-/- up
D
number of genes
p.adjust
positive regulation of defense response
positive regulation of response to external stimulus
regulation of response to biotic stimulus
positive regulation of cytokine production
response to molecule of bacterial origin
cellular response to biotic stimulus
response to bacterium
positive regulation of phagocytosis
phagocytosis
myeloid leukocyte activation
negative regulation of cell activation
negative regulation of immune system process
defense response to symbiont
defense response to virus
response to virus
defense response to Gram-positive bacterium
defense response to bacterium
defense response to protozoan
cellular response to type II interferon
response to type II interferon
response to interferon-beta
cellular response to interferon-beta
production of molecular mediator of immune response
regulation of production of molecular mediator of immune response
cytokine production involved in immune response
regulation of cytokine production involved in immune response
positive regulation of interleukin-6 production
macrophage cytokine production
eosinophil migration
G protein-coupled receptor signaling pathway
cytokine-mediated signaling pathway
myeloid leukocyte migration
leukocyte migration
positive regulation of leukocyte migration
taxis
chemotaxis
regulation of ERK1 and ERK2 cascade
positive regulation of ERK1 and ERK2 cascade
ERK1 and ERK2 cascade
positive regulation of MAPK cascade
positive regulation of vasculature development
positive regulation of angiogenesis
lymphocyte mediated immunity
leukocyte mediated immunity
regulation of leukocyte mediated immunity
immune effector process
regulation of immune effector process
positive regulation of immune effector process
cell killing
positive regulation of cell killing
antigen processing and presentation of peptide antigen
antigen processing and presentation
regulation of adaptive immune response based on somatic recombination of immune receptors built from immunoglobulin superfamily domains
regulation of adaptive immune response
positive regulation of adaptive immune response based on somatic recombination of immune receptors built from immunoglobulin superfamily domains
positive regulation of adaptive immune response
adaptive immune response based on somatic recombination of immune receptors built from immunoglobulin superfamily domains
adaptive immune response
type II interferon production
regulation of type II interferon production
regulation of T cell activation
regulation of leukocyte cell-cell adhesion
leukocyte cell-cell adhesion
regulation of cell-cell adhesion
T cell activation
regulation of lymphocyte activation
regulation of leukocyte activation
positive regulation of leukocyte activation
positive regulation of cell activation
positive regulation of lymphocyte activation
positive regulation of T cell activation
positive regulation of cell adhesion
lymphocyte proliferation
regulation of lymphocyte proliferation
mononuclear cell proliferation
regulation of mononuclear cell proliferation
leukocyte proliferation
regulation of leukocyte proliferation
positive regulation of mononuclear cell proliferation
positive regulation of leukocyte proliferation
FATP1-/- up

A

PLIN2$^{-/-}$ macrophages intracellular *Mtb* DE genes: up 69, down 36

FATP1$^{-/-}$ macrophages intracellular *Mtb* DE genes: up 0, down 0

CPT2$^{-/-}$ macrophages intracellular *Mtb* DE genes: up 3, down 7

B

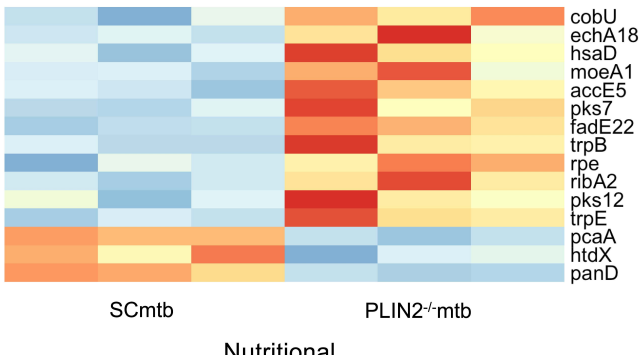

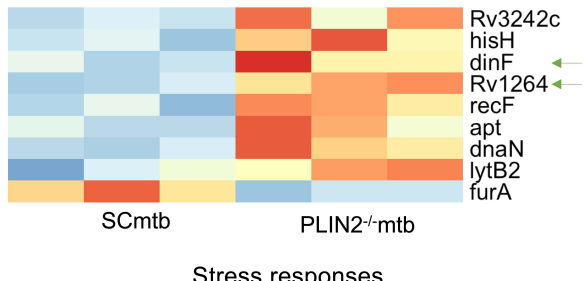

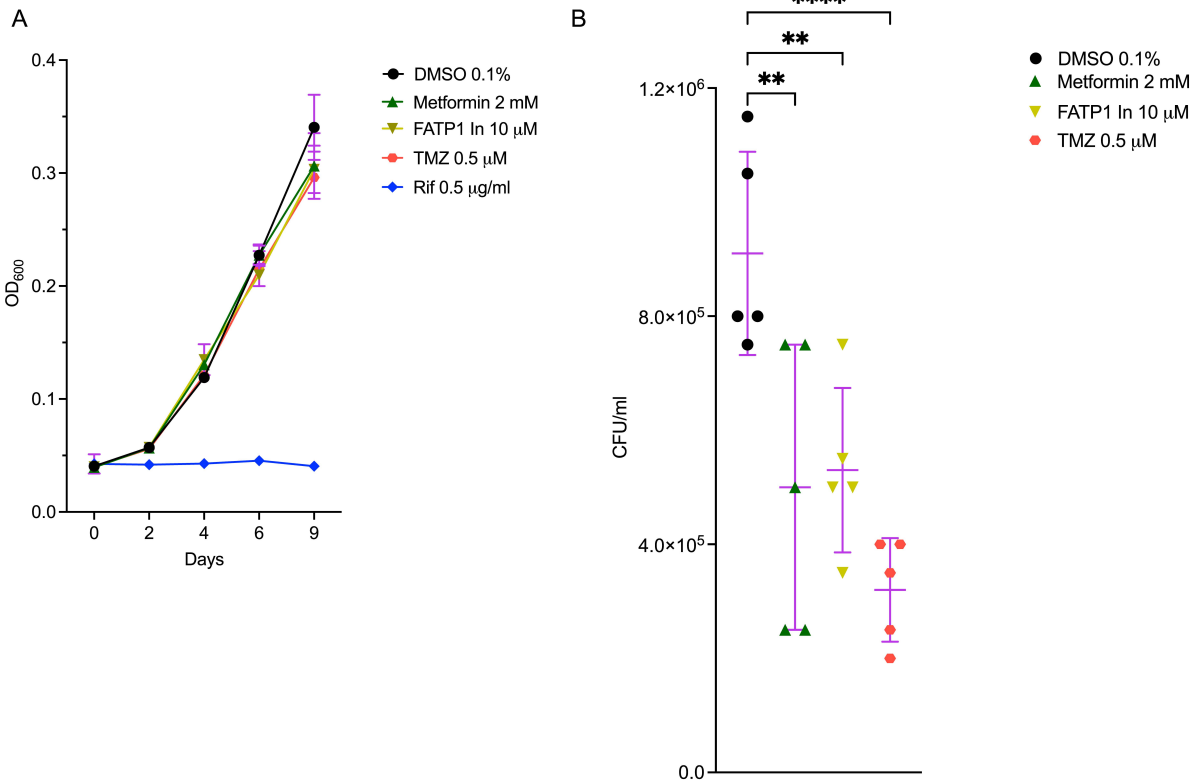
A
0.4
0.3
0.2
0.1
0.0
OD600
0
2
4
6
9
Days
DMSO 0.1%
Metformin 2 mM
FATP1 In 10 μM
TMZ 0.5 μM
Rif 0.5 μg/ml
B
****
**
**
1.2×10^6
8.0×10^5
4.0×10^5
0.0
CFU/ml
DMSO 0.1%
Metformin 2 mM
FATP1 In 10 μM
TMZ 0.5 μM